

Near-unity Light Absorption in a Monolayer WS₂ Van der Waals Heterostructure Cavity

Itai Epstein,^{1,*} Bernat Terrés,^{1,*} André J. Chaves,² Varun-Varma Pusapati,¹ Daniel A. Rhodes,³ Bettina Frank,⁴ Valentin Zimmermann,⁴ Ying Qin,⁵ Kenji Watanabe,⁶ Takashi Taniguchi,⁶ Harald Giessen,⁴ Sefaattin Tongay,⁷ James C. Hone,³ Nuno M. R. Peres,^{8,9} and Frank Koppens^{1,10,†}

¹*ICFO - The Institute of Photonic Sciences, Castelldefels 08860, Barcelona, Spain[‡]*

²*Department of Physics, Instituto Tecnológico de Aeronáutica, DCTA, 12228-900 São José dos Campos, Brazil*

³*Department of Mechanical Engineering, Columbia University, New York, NY 10027*

⁴*4th Physics Institute and Research Center SCoPE, University of Stuttgart, 70569 Stuttgart, Germany*

⁵*School for Engineering of Matter Transport and Energy, Arizona State University Tempe, AZ 85287, USA*

⁶*National Institute for Materials Science, 1-1 Namiki, Tsukuba 305-0044, Japan*

⁷*School for Engineering of Matter Transport and Energy Arizona State University Tempe, AZ 85287, USA*

⁸*Centro de Física and Departamento de Física and QuantaLab, Universidade do Minho, P-4710-057 Braga, Portugal*

⁹*International Iberian Nanotechnology Laboratory (INL), Av. Mestre José Veiga, 4715-330 Braga, Portugal*

¹⁰*ICREA – Institució Catalana de Recerca i Estudis Avançats, Barcelona, Spain*

A direct bandgap and large exciton binding energies provide an optical response dominated by excitons in monolayer transition-metal-dichalcogenides (TMDs). While various approaches have been applied to light-exciton interaction in TMDs, the achieved strength have been far below unity, and a complete picture of its underlying physical mechanisms and fundamental limits has not been provided. Here, we introduce a TMD-based van der Waals heterostructure cavity that provides near-unity excitonic absorption, and excitonic complexes emission that are observed at ultra-low excitation powers. Our results are in full agreement with a quantum theoretical framework introduced to describe the light-exciton-cavity interaction. We find that the subtle interplay between the radiative, non-radiative and dephasing decay rates plays a crucial role, and unveil a universal absorption law for excitons in 2D-systems. This enhanced light-exciton interaction provides a platform for studying excitonic phase-transitions and quantum nonlinearities and paves the way to new possibilities for 2D semiconductor-based optoelectronic devices.

The remarkable properties of excitons in monolayer TMDs, together with the ability to readily control their charge carrier density, have attracted a significant amount of interest in recent years. This has led to the observation of numerous phenomena, such as higher order exciton complexes^{1–4}, coupled spin-valley physics^{5–9}, single photon quantum emitters^{10–14}, together with monolayer semiconductor-based lasers, light-emitting diodes, and photodetectors^{15–19}.

Excitons in monolayer TMDs exhibit strong interaction with light, both in absorption and photoemission processes^{20–23}, which facilitates large photovoltaic response enabled by strong peaks in the joint density of states²⁴ and strong-coupling^{25,26}, to name two examples. Unlike their counterparts in quantum-well semiconductors, excitons in TMDs practically dominate the optical response of the material^{21,22}. This stems from

their large binding energies, which are a result of the strong Coulomb interaction and reduced screening that arise from their low dimensionality²⁷. The existence of robust excitonic states deep within the bandgap results in an optical bandgap that differs significantly from the electronic one²⁸, and thus prevails over the standard electronic-based optical response.

Nevertheless, in absolute values, the absorption of light by excitons in TMDs is far below unity, ranging between 2 – 12% for as-transferred monolayers^{3,29–32}, and about 20 – 30% with the aid of a cavity^{33–35}. Similarly, 5 – 7% absorption have been previously reported for trions^{36,37}. Thus, the question remains whether the achievable interaction strength can be pushed further and what would its limit be? Can unitary absorption be reached by excitons in an atomic thin layer? The answers may play an important role in the understanding of excitonic complexes in TMDs, and the realization of practical 2D material optoelectronic devices.

Here, we demonstrate ultra-strong light-exciton interaction strength in a WS₂-based high quality van der Waals heterostructure cavity (VHC), i.e an optical

* These authors contributed equally

† frank.koppens@icfo.eu

‡ itai.epstein@icfo.eu

cavity built from van der Waals materials, which can be controlled both electrically and optically. The cavity enhances the light field over the TMD due to constructive interferences. While the cavity is quite broadband, the near-unity absorption is attainable owing to four major elements: (1) Achievable narrow excitonic linewidths. (2) The ability to carefully balance the interplay between the radiative and non-radiative decay rates, γ_r and γ_{nr} , respectively. (3) The enhancement of the vacuum radiative decay rate, $\gamma_{r,0}$, via the Purcell factor, shifting the maximum absorption to larger linewidths. (4) Obtaining extremely low dephasing rate, γ_d .

We show that this approach yields a large photo-excited excitonic population, with record values of $\sim 92\%$ excitonic absorption, $\sim 41\%$ for singlet and triplet trion states, and even the observation of the next negatively charged trion state with $\sim 28\%$ absorption. In addition, it enables the observation of biexcitons photoemission at ultra-low continuous-wave (cw) laser powers down to a few nW, which is three orders of magnitude lower than previously reported values³⁸. We introduce an analytical approach to describe the light-exciton-cavity interaction, which is based on the semiconductor Bloch equations combined with a quantum transfer matrix method. The model takes into account the contribution of both the exciton radiative and non-radiative decay rates, γ_r and γ_{nr} , which have already been shown to affect the excitonic coherence and high reflection of monolayer TMDs^{39–41}. In addition, we include the existence of a pure dephasing rate, γ_d , to account for quantum coherence effects as part of the multiple interferences within the cavity. We find that the relation between γ_r and γ_{nr} establishes the condition for maximal absorption, and its limit is set by the value of the pure dephasing rate γ_d , basically limiting the coherence of the system. Experimentally, we control the non-radiative channels with temperature, and the radiative via the geometrical parameters of the VHC (Purcell effect). Finally, we expose the existence of a universal absorption law for excitons in 2D systems in this class of devices.

The VHC is composed of a monolayer WS₂, which is encapsulated by hBN, and transferred on top of a gold back reflector (Fig. 1(a)). We have fabricated two such heterostructure cavities - sample U1 in which we used for the back reflector a single crystalline, atomically flat gold flake⁴², and sample U2, where we used a standard evaporated gold film as the back reflector, which is also used for electrostatic gating. In these structures the transmission is zero, and the absorption can be obtained from $1 - \frac{R}{R_0}$, where R and R_0 are the reflection from the structure with and without the TMD, respectively.

Fig. 1(b) shows the typical absorption spectra, obtained from sample U2, for different gate voltages at $T = 4K$. An absorption value as high as $\sim 85\%$ can be

seen at an energy of $E = 2.08\text{eV}$, corresponding to the WS₂ neutral exciton (X), an absorption value of $\sim 41\%$ at $E = 2.041\text{eV}$, corresponding to both singlet and triplet trions (Tr_t/Tr_s) (see SI), and an absorption value of $\sim 28\%$ at $E = 2.023\text{eV}$, corresponding to the next charged state of the trion (X^{--}). All energetic positions and separations are in agreement with previous reports on WS₂^{4,43}. In principle, by changing the gate voltage we control the charge carriers in the WS₂, and thus the relative spectral weights of (X), (Tr) and (X^{--})^{36,44}, i.e., the absorption spectrum can be controlled electrically. To the best of our knowledge, these are record values together with the first observation of the X^{--} peak in an absorption spectra of TMDs, and are a direct result of the strong light-matter interaction provided by the VHC.

To study the ultimate absorption limits, we vary the temperature which controls the excitonic linewidth, as presented in Fig. 1(c) and (d). While the exciton linewidth shows a continuous decrease with decreasing temperature (Fig. 1(d) red curve), as known for the ground state exciton in semiconductors⁴⁵ and TMDs^{46,47}, the excitonic absorption shows a non-monotonic temperature dependency. An absorption value of $\sim 55\%$ can already be seen at room-temperature, which increases to a maximum value of $\sim 92\%$ at $T = 110K$, and then decreases rapidly to $\sim 77\%$ at $T = 4K$ (Fig. 1(d) blue curve), the low temperature limit of our cryostat.

In order to understand the physical origin of this behavior, we developed a theoretical formalism that combines an equation of motion method for the exciton (described by bosonic operators), which is similar to the well-known (interacting) Bloch equations^{48,49}, together with a quantum treatment of the cavity using a quantum transfer matrix method (QTMM) (see SI). To take into account the quantum nature of the pure dephasing, the QTMM treats the electromagnetic fields as operators, rather than classical fields. This provides the relation between the polarization operator and the field in the 2D material. The solution, which describes the optical response of the TMD, leads to the an Elliott-type formula appropriate for the 2D material⁴⁹. This allows us to calculate the absorption, via the reflection operator's expectation value, taking into account the contributions of both the $\gamma_{r,0}$ (and its Purcell enhancement), γ_{nr} , and γ_d . The latter is a purely quantum effect that is important to consider due to the multiple interferences in the cavity, making the absorption sensitive to exciton dephasing³⁹.

Following this approach (see SI), the maximum absorption can then be approximated by:

$$A_{\max} = \xi_1 \frac{\gamma_{r,0}}{\gamma_T} \left[1 - \xi_2 \left(1 + 2 \frac{\gamma_d}{\gamma_T} \right) \frac{\gamma_{r,0}}{\gamma_T} \right], \quad (1)$$

with

$$\gamma_T = \gamma_{nr} + 2\gamma_d + \zeta\gamma_{r,0}, \quad (2)$$

where $\frac{\gamma_{r,0}}{\gamma_T}$ and $\frac{\gamma_d}{\gamma_T}$ are the normalized vacuum radiative decay and dephasing, and the coefficients ξ_1 , ξ_2 , and ζ are (see SI) parameters depending on the geometry, defined by the sizes and dielectric functions composing the different parts of the cavity, with ζ representing the Purcell factor, and $\gamma_r = \zeta\gamma_{r,0}$ being the renormalized radiative decay rate.

To expose the roles of the different decay rates in the absorption behavior, we show in Fig. 2(a) the calculated absorption dependence on the exciton linewidth for several dephasing values. For each γ_d , $\gamma_{r,0}$ is kept constant, as it does not depend on temperature, and we vary γ_{nr} (solid lines). For the simple case of negligible γ_d , we obtain a matching condition for the maximum absorption point: $\gamma_{nr} \approx \zeta\gamma_{r,0}$ (see SI), and 100% absorption. This implies that the relation between γ_r , and γ_{nr} , rather than their absolute values, sets the matching condition for maximal absorption, and γ_d sets the limit of the absolute achievable absorption when the matching condition is fulfilled. For comparison, the absorption of a suspended monolayer is presented for the same dephasing values (dashed curves), exhibiting the same behavior and showing the known maximal absorption limit of 50% for a suspended monolayer⁵⁰.

It can be seen that the VHC not only enables near-unity absorption, but owing to the Purcell effect, also shifts its to larger total linewidths, enabling the experimental realization of such large absorption. For the more general case including finite dephasing, the matching condition translates to the more complex relation between $\frac{\gamma_{r,0}}{\gamma_T}$ and $\frac{\gamma_d}{\gamma_T}$ (Fig. 2(b)). A ternary plot of the absorption as function of the normalized radiative, nonradiative and pure dephasing decay rates, is presented in Fig. 2(b), showing all the possibilities in the decay rates' space. It can be seen from (Fig. 2(a)) that away from the matching condition, the dephasing has little effect and the absorption decreases following two different regimes. For very small γ_T , $\gamma_{r,0}$ dominates the linewidth and the absorption decreases as the TMD becomes highly reflective (corresponding to negative absorption, as seen in (Fig. 2(b)))^{39–41}. For very large γ_T , the non-radiative and dephasing dominates the linewidth and the absorption is decreased as the TMD becomes transparent.

The above discussed decay rates will change significantly for different cavity designs, TMD quality, fabrication-induced interface quality, and can vary locally⁴⁰. Yet, via a simple representation of Eq. 1 as function of γ_T^{-1} , the model makes a striking prediction and inescapable universal feature of this class of devices:

$$\frac{A_{\max}\gamma_T}{\xi_1} = \gamma_{r,0} \left[1 - \xi_2 \left(1 + 2\frac{\gamma_d}{\gamma_T} \right) \frac{\gamma_{r,0}}{\gamma_T} \right]. \quad (3)$$

e.g. this implies a linear relationship between $A_{\max}\gamma_T/\xi_1$ and $1/\gamma_T$, provided that $\gamma_d/\gamma_T \ll 1$. Indeed, the universal law is confirmed by the experimental data from different samples and locations presented in Fig. 2(c). The different samples follow their own straight line, which encodes their different quality, but the generic behavior is the same for all. In addition, $\gamma_{r,0}$ of the different samples can be extracted from the (extrapolated) crossing point $1/\gamma_T = 0$. In principle, this universal law should hold for any 2D excitonic system where $\gamma_d \ll \gamma_T$.

Another important outcome of this analysis is the ability to compare different excitonic properties via their absorption response. Fig. 2(d) shows the extracted temperature dependent γ_{nr} and γ_d (see SI) and their phenomenological fit^{39,47}, for the same samples and in Fig. 2(c). These correlate directly with their absorption behavior, indicating that higher dephasing leads to lower absorption.

The light passing through the heterostructure with a back reflector can be regarded as an asymmetric Fabry-Perot cavity. The simplest case of such a cavity is a single dielectric layer on top of a mirror, known as the Salisbury screen, and when the thickness of the dielectric is chosen to be a quarter wavelength of the light in the dielectric, constructive interference takes place on the surface of the dielectric and the field is locally enhanced. Owing to the penetration depth into the gold mirror, the bottom hBN thickness is less than the quarter wavelength, and the top hBN is then optimized. Specifically for the VHC, the situation is more complex, owing to the contributions from the multiple-layer structure and the gold mirror. Basically, the tunable properties of the TMD act as a layer within the cavity itself, which can be either absorptive or reflective, as explained before. On the other hand, the cavity provides a degree of freedom to balance the matching condition in order to achieve strong light-exciton interaction.

In the same manner we have designed the heterostructure cavity for maximal interaction strength, it can be designed to any intermediate value by changing the VHC design. It can also be designed to completely turn off the interaction between the light and the TMD, for example. The spatial distribution of the absorption at $T = 300K$ of such a design is presented in Fig. 3(a), where on the same device we fabricated two different cavities, one in which the interaction is maximal, defined as "on", and in the other the interaction is turned "off" completely (Fig. 3 Inset). This is done by adding another hBN flake below a part of the heterostructure. In Fig. 3(b) we show the extracted exciton linewidth distribution of Fig. 3(a). The spatial correlation between the absorption and linewidth can be directly observed in the "on" areas of the two figures, e.g., lower linewidth correlates to higher absorption, which is indeed the case for $T = 300K$ (see Fig. 1(d)). The source of the

spatial distribution comes from the inhomogeneity of the sample, a well known issue in TMDs⁴⁰. Furthermore, the extracted radiative decay rates from the two cavities corresponds to a change of $\zeta\gamma_{r,0}$ from $\sim 2.2\text{meV}$ in the "on" region to $\sim 70\mu\text{eV}$ in the "off" region, in agreement of the linewidth modulation obtained by Ref⁵¹.

The ability to achieve unitary excitonic absorption implies that a large photo-excited excitonic density can be obtained while maintaining low excitation power. It was already shown that TMD's are highly affected by the excitation power, resulting in either heating effects that changes the excitonic properties temporarily⁵², or permanent effects that completely alter the material's response, such as optical doping and environmental surface interactions^{3,53}. Yet, this challenging and desirable high exciton density plays a major role in several physical phenomena, such as Bosonic condensation, phase transitions⁵⁴ and biexcitons emission³, for example. The formation of biexcitons is directly related to the formed excitonic density and thus also to the possible appearance of the biexciton peak in the photoluminescence (PL) spectrum³. The predicted intensity relation between the exciton and biexciton emission is in the form of the power law $I_{XX} = I_X^\alpha$, with α ranging between 1.2 – 1.9 due to lack of thermal equilibrium³. Thus, the latter can be used to probe the efficiency of exciton photo-generation in the VHC, as compared to a naive calculation based solely on the light source's attributes.

Fig. 4(a) shows the PL spectra, normalized to the exciton emission intensity (I_X), obtained from the VHC for different cw excitation powers. Several peaks can be observed and are marked as X - exciton at $E = 2.071\text{eV}$, Tr_t/Tr_s - singlet/triplet trions⁴³ at $2.034\text{eV}/2.04\text{eV}$, respectively, and XX - biexciton at $E = 2.018\text{eV}$. Remarkably, the XX emission peak can be observed at excitations powers down to few nW. This excitation power is three orders of magnitude smaller than the lowest previously reported for biexcitons³⁸. Actually, at powers over $\sim 30\mu\text{W}$ the XX emission intensity is so high that it saturates our detection device. Fig. 4(b) shows the power law analysis of the I_{XX} and I_X peaks, and the obtained $\alpha = 1.62$ for I_{XX} provides a confirmation for the identity of the biexciton. Based on the illumination attributes in our experimental conditions, the maximal used power of $\sim 400\mu\text{W}$ yields a calculated excitonic density of $\sim 2.5 \cdot 10^{11}[\text{cm}^{-2}]$. This exciton density is 2 orders of magnitude larger than what was achieved in previous works using CW excitations, and is similar to densities obtained using ultrafast laser pulses²⁹. While it is possible that at high cw excitation powers heating effects may kick in, using pulsed excitation (as in ref²⁹ for example) with our VHC, one can obtain an excitonic density of $\sim 5 \cdot 10^{13}[\text{cm}^{-2}]$ with little heating, as compared to $\sim 6.4 \cdot 10^{12}[\text{cm}^{-2}]$.

In conclusion, the new type of optical cavity presented here, which is based solely on van der Waals heterostructures, is designed for strong light-exciton interaction, and unveils a universal absorption law for excitons in 2D systems. This enhanced light-exciton interaction can act as a platform for probing quantum nonlinear dynamics of excitons^{39,41} and their state of matter⁵⁴, and paves the way efficient optoelectronic devices, such as, detectors, modulators and optically-pumped light emitting devices, based on monolayer semiconductors.

METHODS

Optical setup All temperature measurements were done in an Attodry800 cryostat, and spectral detection with an Andor spectrometer. A white light source was used for the reflection measurements and a 532nm laser for the PL. The light was focused using a Nikon objective with $NA = 0.6$.

Synthesis (sample U2) WS_2 was grown using chemical vapor transport with a WCl_6 precursor in excess sulfur. W, 99.999 %, and sulfur (99.9995 %) were first loaded into a quartz ampoule in a 1:2, W:S, ratio with an additional excess of 24 mg/cm^3 of sulfur. 60 mg of WCl_6 was added into the quartz ampoule inside of a nitrogen glovebox, the ampoule was then removed from the glovebox and quickly pumped down to 5×10^{-5} Torr to avoid deterioration of the WCl_6 . The ampoule was then sealed under vacuum. The reagents were subsequently heated to 1000°C within 24 h and with a 100°C temperature gradient between the hot and cold zone. The ampoule was then allowed to dwell at this temperature for 2 weeks before being cooled to 400°C over an additional 2 weeks. The as harvested crystals were then rinsed in acetone and isopropanol and dried in air before being used.

Device Fabrication Monolayer flakes of WS_2 were mechanically exfoliated from the aforementioned single crystals on to 285 nm SiO_2 chip. On a separate chip, hexagonal boron nitride (hBN) was exfoliated and picked up using a dry transfer, PDMS/polypropylene carbonate (PPC) stamp method mounted on to a glass slide. Subsequently the hBN is used to pick up, in order, two few-layer graphene contacts, the monolayer WS_2 , and an underlying hBN. The final stack is then transferred on to a the gold pad at 125°C and rinsed in acetone overnight.

AUTHOR CONTRIBUTION

I.E. conceived the idea, performed simulations, experiments and analysis of the results. B.T fabricated samples and analyzed the results. A.C. and N.P introduced the theoretical framework and simulations. D.R., B.F., V.Z., Y.Q, K.W., T.T., H.G., S.T., and J.H. supplied materials

and/or samples. F.K. supervised the work. All authors contributed to discussions and writing of the manuscript.

ACKNOWLEDGMENTS

S.T acknowledges support from NSF DMR-1552220 and DMR-1838443. NMRP acknowledges financing from Eu-

ropean Commission through the project "Graphene-Driven Revolutions in ICT and Beyond" (Ref. No. 785219) and from FEDER and the Portuguese Foundation for Science and Technology (FCT) through project POCI-01-0145- FEDER-028114. H.G. and B.F. acknowledge support from ERC advanced grant COMPLEXPLAS.

- ¹ Mak, K. F. *et al.* Tightly bound trions in monolayer MoS₂. *Nature Materials* **12**, 207–211 (2013). URL <http://www.nature.com/articles/nmat3505>.
- ² Ross, J. S. *et al.* Electrical control of neutral and charged excitons in a monolayer semiconductor. *Nature Communications* **4**, 1474 (2013). URL <http://www.nature.com/articles/ncomms2498>.
- ³ You, Y. *et al.* Observation of biexcitons in monolayer WSe₂. *Nature Physics* **11**, 477–481 (2015). URL <http://www.nature.com/articles/nphys3324>.
- ⁴ Plechinger, G. *et al.* Identification of excitons, trions and biexcitons in single-layer WS₂. *physica status solidi (RRL) - Rapid Research Letters* **9**, 457–461 (2015). URL <http://doi.wiley.com/10.1002/pssr.201510224>.
- ⁵ Xiao, D., Liu, G.-B., Feng, W., Xu, X. & Yao, W. Coupled Spin and Valley Physics in Monolayers of MoS₂ and Other Group-VI Dichalcogenides. *Physical Review Letters* **108**, 196802 (2012). URL <https://link.aps.org/doi/10.1103/PhysRevLett.108.196802>.
- ⁶ Zeng, H., Dai, J., Yao, W., Xiao, D. & Cui, X. Valley polarization in MoS₂ monolayers by optical pumping. *Nature Nanotechnology* **7**, 490–493 (2012). URL <http://www.nature.com/articles/nnano.2012.95>.
- ⁷ Mak, K. F., He, K., Shan, J. & Heinz, T. F. Control of valley polarization in monolayer MoS₂ by optical helicity. *Nature Nanotechnology* **7**, 494–498 (2012). URL <http://www.nature.com/articles/nnano.2012.96>.
- ⁸ Cao, T. *et al.* Valley-selective circular dichroism of monolayer molybdenum disulphide. *Nature Communications* **3**, 887 (2012). URL <http://www.nature.com/articles/ncomms1882>.
- ⁹ Xu, X., Yao, W., Xiao, D. & Heinz, T. F. Spin and pseudospins in layered transition metal dichalcogenides. *Nature Physics* **10**, 343–350 (2014). URL <http://www.nature.com/articles/nphys2942>.
- ¹⁰ Tonndorf, P. *et al.* Single-photon emission from localized excitons in an atomically thin semiconductor. *Optica* **2**, 347 (2015). URL <https://www.osapublishing.org/abstract.cfm?URI=optica-2-4-347>.
- ¹¹ Chakraborty, C., Kinnischtzke, L., Goodfellow, K. M., Beams, R. & Vamivakas, A. N. Voltage-controlled quantum light from an atomically thin semiconductor. *Nature Nanotechnology* **10**, 507–511 (2015). URL <http://www.nature.com/articles/nnano.2015.79>.
- ¹² Koperski, M. *et al.* Single photon emitters in exfoliated WSe₂ structures. *Nature Nanotechnology* **10**, 503–506 (2015). URL <http://www.nature.com/articles/nnano.2015.67>.
- ¹³ He, Y.-M. *et al.* Single quantum emitters in monolayer semiconductors. *Nature Nanotechnology* **10**, 497–502 (2015). URL <http://www.nature.com/articles/nnano.2015.75>.
- ¹⁴ Srivastava, A. *et al.* Optically active quantum dots in monolayer WSe₂. *Nature Nanotechnology* **10**, 491–496 (2015). URL <http://www.nature.com/articles/nnano.2015.60>.
- ¹⁵ Radisavljevic, B., Radenovic, A., Brivio, J., Giacometti, V. & Kis, A. Single-layer MoS₂ transistors. *Nature Nanotechnology* **6**, 147–150 (2011). URL <http://www.nature.com/articles/nnano.2010.279>.
- ¹⁶ Yin, Z. *et al.* Single-Layer MoS₂ Phototransistors. *ACS Nano* **6**, 74–80 (2012). URL <http://pubs.acs.org/doi/10.1021/nm2024557>.
- ¹⁷ Lopez-Sanchez, O., Lembke, D., Kayci, M., Radenovic, A. & Kis, A. Ultrasensitive photodetectors based on monolayer MoS₂. *Nature Nanotechnology* **8**, 497–501 (2013). URL <http://www.nature.com/articles/nnano.2013.100>.
- ¹⁸ Baugher, B. W. H., Churchill, H. O. H., Yang, Y. & Jarillo-Herrero, P. Optoelectronic devices based on electrically tunable p–n diodes in a monolayer dichalcogenide. *Nature Nanotechnology* **9**, 262–267 (2014). URL <http://www.nature.com/articles/nnano.2014.25>.
- ¹⁹ Ross, J. S. *et al.* Electrically tunable excitonic light-emitting diodes based on monolayer WSe₂ p–n junctions. *Nature Nanotechnology* **9**, 268–272 (2014). URL <http://www.nature.com/articles/nnano.2014.26>.
- ²⁰ Mak, K. F. & Shan, J. Photonics and optoelectronics of 2D semiconductor transition metal dichalcogenides. *Nature Photonics* **10**, 216–226 (2016). URL <http://www.nature.com/articles/nphoton.2015.282>.
- ²¹ Wang, G. *et al.* Colloquium: Excitons in atomically thin transition metal dichalcogenides. *Reviews of Modern Physics* **90**, 021001 (2018). URL <https://link.aps.org/doi/10.1103/RevModPhys.90.021001>.
- ²² Mueller, T. & Malic, E. Exciton physics and device application of two-dimensional transition metal dichalcogenide semiconductors. *npj 2D Materials and Applications* **2**, 29 (2018). URL <http://www.nature.com/articles/s41699-018-0074-2>.
- ²³ Wurstbauer, U., Miller, B., Parzinger, E. & Holleitner, A. W. Light-matter interaction in transition metal dichalcogenides and their heterostructures. *Journal of Physics D: Applied Physics* **50**, 173001 (2017). URL <http://stacks.iop.org/0022-3727/50/i=17/a=173001?key=crossref.f730cf2e4c82939dce6e4a6289cf7606>.
- ²⁴ Britnell, L. *et al.* Strong Light-Matter Interactions in Heterostructures of Atomically Thin Films. *Science* **340**, 1311 LP – 1314 (2013). URL <http://science.sciencemag.org/content/340/6138/1311.abstract>.

- ²⁵ Liu, X. *et al.* Strong light-matter coupling in two-dimensional atomic crystals. *Nature Photonics* **9**, 30–34 (2015). URL <http://www.nature.com/articles/nphoton.2014.304>.
- ²⁶ Schneider, C., Glazov, M. M., Korn, T., Höfling, S. & Urbaszek, B. Two-dimensional semiconductors in the regime of strong light-matter coupling. *Nature Communications* **9**, 2695 (2018). URL <http://www.nature.com/articles/s41467-018-04866-6>.
- ²⁷ Chernikov, A. *et al.* Exciton Binding Energy and Nonhydrogenic Rydberg Series in Monolayer WS₂. *Physical Review Letters* **113**, 076802 (2014). URL <https://link.aps.org/doi/10.1103/PhysRevLett.113.076802>.
- ²⁸ Ugeda, M. M. *et al.* Giant bandgap renormalization and excitonic effects in a monolayer transition metal dichalcogenide semiconductor. *Nature Materials* **13**, 1091–1095 (2014). URL <http://www.nature.com/articles/nmat4061>.
- ²⁹ Poellmann, C. *et al.* Resonant internal quantum transitions and femtosecond radiative decay of excitons in monolayer WSe₂. *Nature Materials* **14**, 889–893 (2015). URL <http://www.nature.com/articles/nmat4356>.
- ³⁰ Robert, C. *et al.* Exciton radiative lifetime in transition metal dichalcogenide monolayers. *Physical Review B* **93**, 205423 (2016). URL <https://link.aps.org/doi/10.1103/PhysRevB.93.205423>.
- ³¹ Okada, M. *et al.* Observation of biexcitonic emission at extremely low power density in tungsten disulfide atomic layers grown on hexagonal boron nitride. *Scientific Reports* **7**, 322 (2017). URL <http://www.nature.com/articles/s41598-017-00068-0>.
- ³² Li, Y. *et al.* Measurement of the optical dielectric function of monolayer transition-metal dichalcogenides: MoS₂, MoSe₂, WS₂, and WSe₂. *Physical Review B* **90**, 205422 (2014). URL <https://link.aps.org/doi/10.1103/PhysRevB.90.205422>.
- ³³ Bahauddin, S. M., Robotjazi, H. & Thomann, I. Broadband Absorption Engineering to Enhance Light Absorption in Monolayer MoS₂. *ACS Photonics* **3**, 853–862 (2016). URL <http://pubs.acs.org/doi/10.1021/acsp Photonics.6b00081>.
- ³⁴ Liu, J.-T., Wang, T.-B., Li, X.-J. & Liu, N.-H. Enhanced absorption of monolayer MoS₂ with resonant back reflector. *Journal of Applied Physics* **115**, 193511 (2014). URL <http://aip.scitation.org/doi/10.1063/1.4878700>.
- ³⁵ Wang, Q. *et al.* Fabry–Perot Cavity-Enhanced Optical Absorption in Ultrasensitive Tunable Photodiodes Based on Hybrid 2D Materials. *Nano Letters* **17**, 7593–7598 (2017). URL <http://pubs.acs.org/doi/10.1021/acs.nanolett.7b03579>.
- ³⁶ Mak, K. F. *et al.* Tightly bound trions in monolayer MoS₂. *Nature Materials* **12**, 207–211 (2013). URL <http://www.nature.com/articles/nmat3505>.
- ³⁷ Zhang, C., Wang, H., Chan, W., Manolatu, C. & Rana, F. Absorption of light by excitons and trions in monolayers of metal dichalcogenide MoS₂: Experiments and theory. *Physical Review B* **89**, 205436 (2014). URL <https://link.aps.org/doi/10.1103/PhysRevB.89.205436>.
- ³⁸ Ye, Z. *et al.* Efficient generation of neutral and charged biexcitons in encapsulated WSe₂ monolayers. *Nature Communications* **9**, 3718 (2018). URL <http://www.nature.com/articles/s41467-018-05917-8>.
- ³⁹ Scuri, G. *et al.* Large Excitonic Reflectivity of Monolayer MoSe₂ Encapsulated in Hexagonal Boron Nitride. *Physical Review Letters* **120**, 037402 (2018). URL <https://link.aps.org/doi/10.1103/PhysRevLett.120.037402>.
- ⁴⁰ Back, P., Zeytinoglu, S., Ijaz, A., Kroner, M. & Imamoglu, A. Realization of an Electrically Tunable Narrow-Bandwidth Atomically Thin Mirror Using Monolayer MoSe₂. *Physical Review Letters* **120**, 037401 (2018). URL <https://link.aps.org/doi/10.1103/PhysRevLett.120.037401>.
- ⁴¹ Zeytinoglu, S., Roth, C., Huber, S. & Imamoglu, A. Atomically thin semiconductors as nonlinear mirrors. *Physical Review A* **96**, 031801 (2017). URL <https://link.aps.org/doi/10.1103/PhysRevA.96.031801>.
- ⁴² Frank, B. *et al.* Short-range surface plasmonics: Localized electron emission dynamics from a 60-nm spot on an atomically flat single-crystalline gold surface. *Science Advances* **3**, e1700721 (2017). URL <http://advances.sciencemag.org/lookup/doi/10.1126/sciadv.1700721>.
- ⁴³ Plechinger, G. *et al.* Trion fine structure and coupled spin-valley dynamics in monolayer tungsten disulfide. *Nature Communications* **7**, 12715 (2016). URL <http://www.nature.com/articles/ncomms12715>.
- ⁴⁴ Paur, M. *et al.* Electroluminescence from multiparticle exciton complexes in transition metal dichalcogenide semiconductors. *Nature Communications* **10**, 1709 (2019). URL <http://www.nature.com/articles/s41467-019-09781-y>.
- ⁴⁵ Rudin, S., Reinecke, T. L. & Segall, B. Temperature-dependent exciton linewidths in semiconductors. *Physical Review B* **42**, 11218–11231 (1990). URL <https://link.aps.org/doi/10.1103/PhysRevB.42.11218>.
- ⁴⁶ Cadiz, F. *et al.* Excitonic Linewidth Approaching the Homogeneous Limit in MoS₂-Based van der Waals Heterostructures. *Physical Review X* **7**, 021026 (2017). URL <http://link.aps.org/doi/10.1103/PhysRevX.7.021026>.
- ⁴⁷ Selig, M. *et al.* Excitonic linewidth and coherence lifetime in monolayer transition metal dichalcogenides. *Nature Communications* **7**, 13279 (2016). URL <http://www.nature.com/articles/ncomms13279>.
- ⁴⁸ Combescot, M., Betbeder-Matibet, O. & Leuenberger, M. N. Analytical approach to semiconductor Bloch equations. *EPL (Europhysics Letters)* **88**, 57007 (2009). URL <http://stacks.iop.org/0295-5075/88/i=5/a=57007?key=crossref.3ec18f06b184f75fb4bdf4aeb02d69c>.
- ⁴⁹ Chaves, A. J., Ribeiro, R. M., Frederico, T. & Peres, N. M. R. Excitonic effects in the optical properties of 2D materials: an equation of motion approach. *2D Materials* **4**, 025086 (2017). URL <http://stacks.iop.org/2053-1583/4/i=2/a=025086?key=crossref.c3d3000a1d03b920a2ae5b877bc1be6b>.
- ⁵⁰ Thongrattanasiri, S., Koppens, F. H. L. & García de Abajo, F. J. Complete Optical Absorption in Periodically Patterned Graphene. *Physical Review Letters* **108**, 047401 (2012). URL <https://link.aps.org/doi/10.1103/PhysRevLett.108.047401>.
- ⁵¹ Fang, H. *et al.* Control of the Exciton Radiative Lifetime in van der Waals Heterostructures. *Physical Review Letters* **123**, 067401 (2019). URL <https://link.aps.org/doi/10.1103/PhysRevLett.123.067401>.
- ⁵² Currie, M., Hanbicki, A. T., Kioseoglou, G. & Jonker, B. T. Optical control of charged exciton states in tungsten disulfide. *Applied Physics Letters* **106**, 201907 (2015). URL <http://aip.scitation.org/doi/10.1063/1.4921472>.

- ⁵³ Cadiz, F. *et al.* Ultra-low power threshold for laser induced changes in optical properties of 2D molybdenum dichalcogenides. *2D Materials* **3**, 045008 (2016). URL <http://stacks.iop.org/2053-1583/3/i=4/a=045008?key=crossref.0970dbdfe74a31e4c3b2c4cb53441d0c>.
- ⁵⁴ Arp, T. B., Pleskot, D., Aji, V. & Gabor, N. M. Electron-hole liquid in a van der Waals heterostructure photocell at room temperature. *Nature Photonics* **13**, 245–250 (2019). URL <http://www.nature.com/articles/s41566-019-0349-y>.

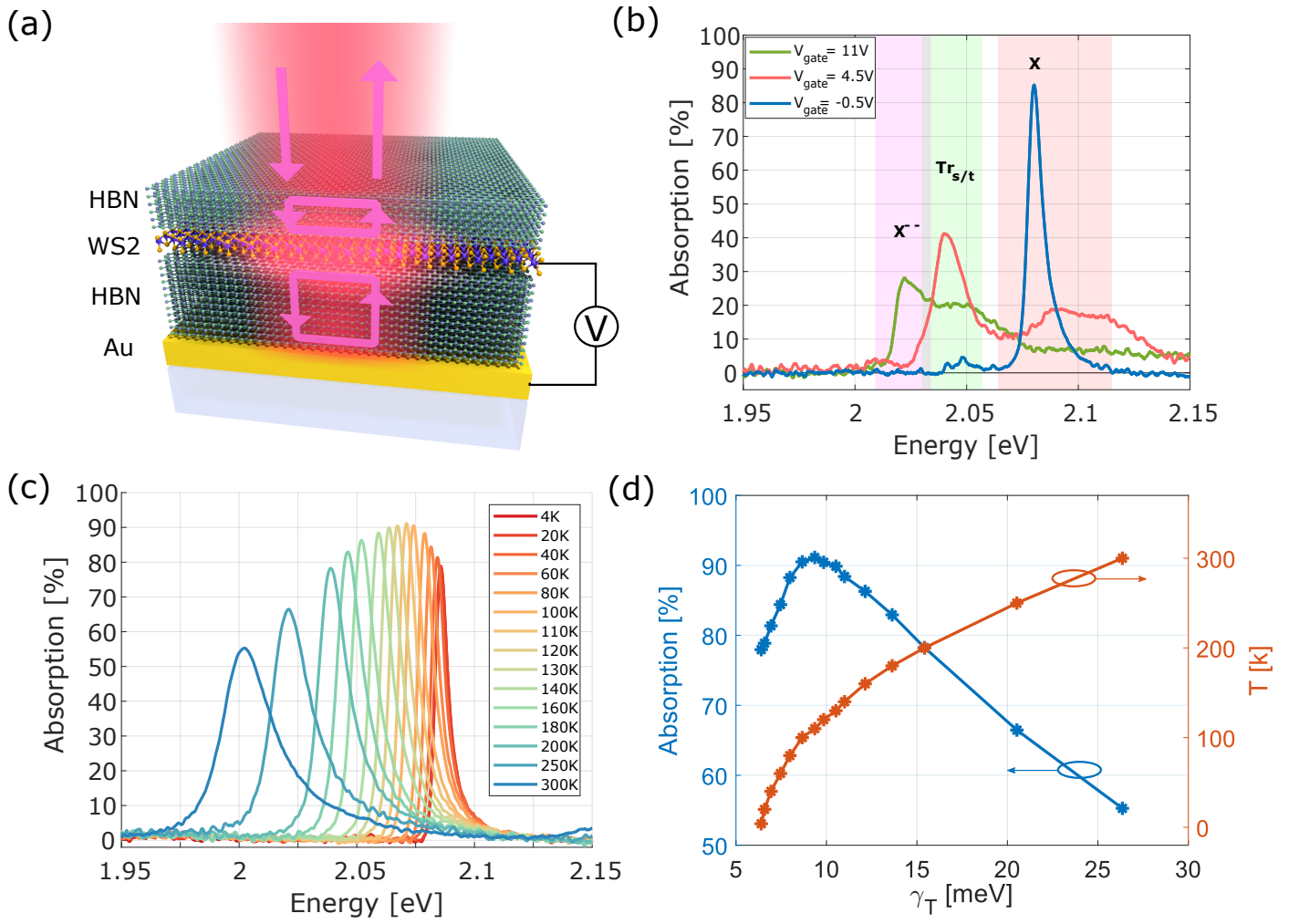


FIG. 1. Light-exciton interaction in the van der Waals heterostructure cavity. (a) The structure of the VHC - an hBN/monolayer WS₂/ hBN heterostructure with optimized hBN thicknesses is transferred on top of a gold back reflector. (b) Gate dependent spectral absorption for sample U2, showing $\sim 85\%$ excitonic absorption, $\sim 41\%$ Trion absorption, and $\sim 28\%$ of the next negatively charged Trion state. (c) Temperature dependent excitonic spectral absorption from sample U1, showing the non-trivial behavior of the absorption, and a maximal absorption value of $\sim 92\%$ at 110K . (d) The maximum excitonic absorption dependency on the total linewidth γ_T (blue curve) and the temperature dependent exciton linewidth (red curve).

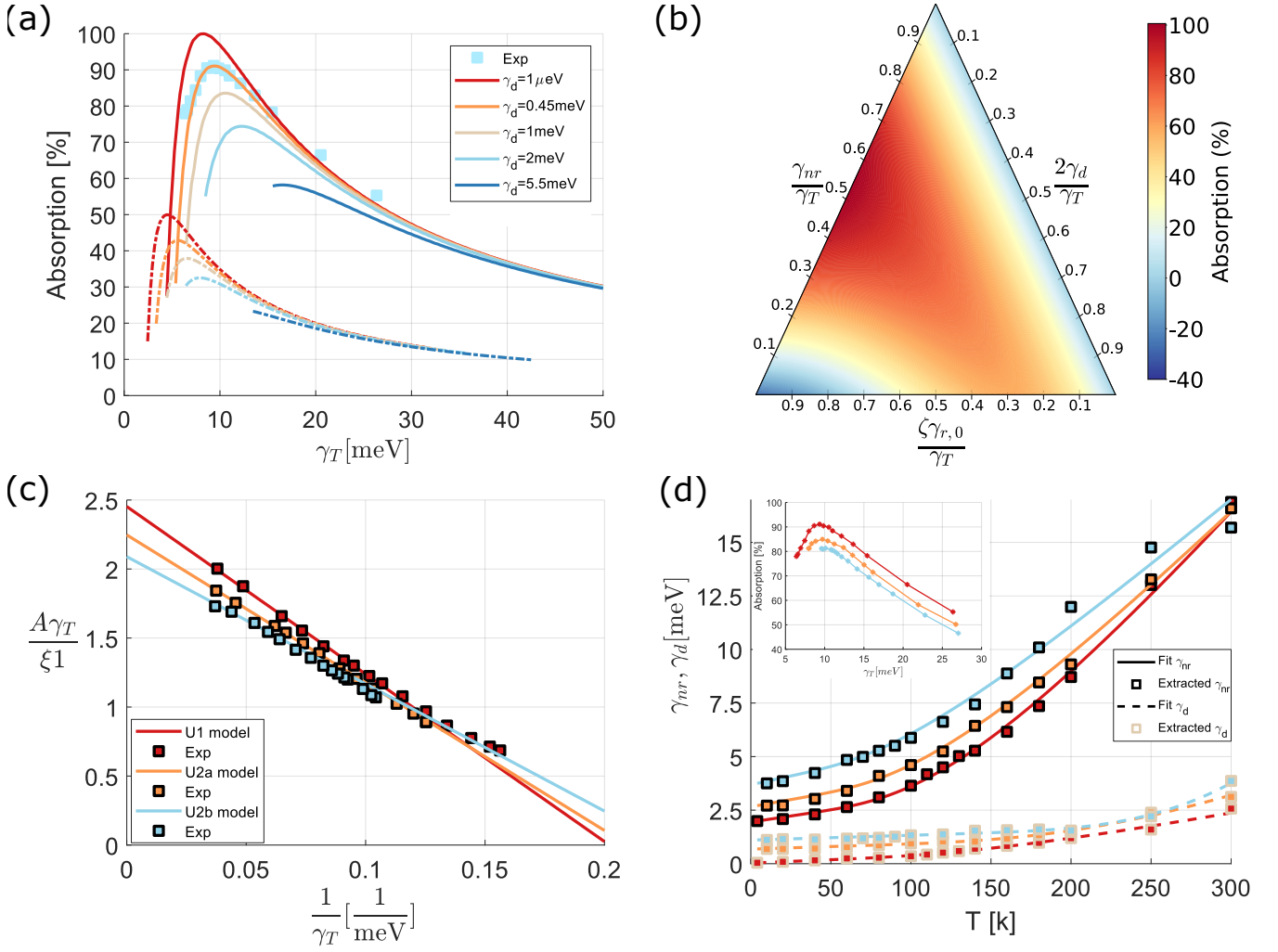


FIG. 2. **Analytical modeling of the light-exciton-cavity interaction.** (a) Calculated absorption dependency on γ_T , for the VHC (solid colors) and a suspended layer (dashed colors), for several dephasing values. The squares show the experimental results from sample U1. (b) Calculated maximal absorption as function of the three normalized radiative decay rates. 100% absorption is achieved when $\gamma_d = 0$ and $\zeta\gamma_{r,0} \approx \gamma_{nr}$. The negative absorption observed at the bottom left corner is due to the dominance of γ_r . (c) Temperature dependent experimental results for the two different samples, U1 and U2, fitted with Eq. 3 exhibiting the universal absorption law. The different radiative decay rate can also be seen at the crossing of the y axis. (d) Extracted γ_{nr} and γ_d and their phenomenological fit, exhibiting the correlation between the achievable absorption and the decay rates. U2a and U2b are different locations on sample U2 that were chosen due to different values of the total linewidth at 4K.

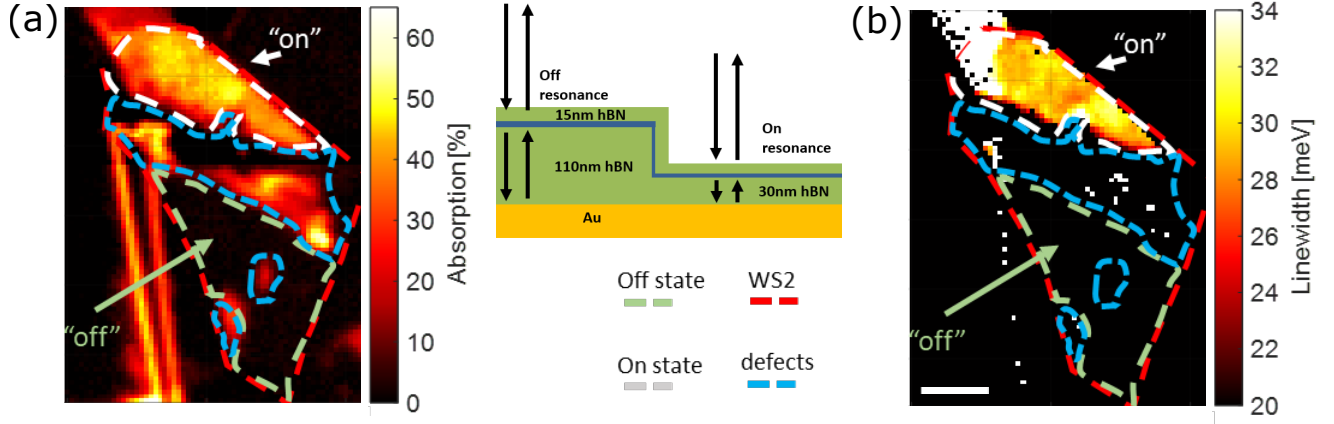


FIG. 3. **Tuning the excitonic optical response via the geometrical design of the VHC.** (a) Spatial distribution of the absorption at room temperature showing the "on" state at the area of maximal interaction and "off" state at the area of minimal interaction. (b) Spatial distribution of the measured linewidth of the excitonic absorption in (a), showing a clear correlation between linewidth and absorption. The scale bar is $5\mu\text{m}$. The inset shows the structure of the sample with two different bottom hBN thicknesses.

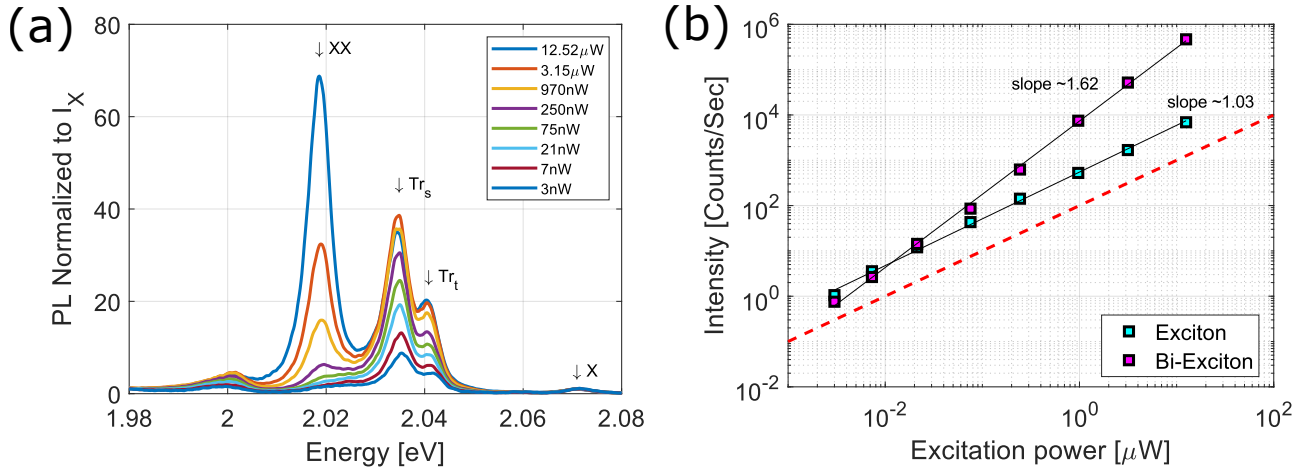


FIG. 4. **Extremely efficient Biexciton emission.** (a) Normalized PL for different CW excitation power ranging from μW to nW. (b) Linear fits of the exciton and Biexciton PL emission showing the superlinear behavior of the Biexcitons peak. The dashed red line correspond to slope = 1.